bioRxiv preprint doi: https://doi.org/10.1101/2021.05.10.443480; this version posted May 10, 2021. The copyright holder for this preprint (which was not certified by peer review) is the author/funder. All rights reserved. No reuse allowed without permission.

Convergent use of phosphatidic acid for Hepatitis C virus and SARS-CoV-2 replication organelle formation

Keisuke Tabata[1†*], Vibhu Prasad[1*], David Paul[1‡], Ji-Young Lee[1], Minh-Tu Pham[1], Woan-Ing Twu[1], Christopher J. Neufeldt[1], Mirko Cortese[1], Berati Cerikan[1], Cong Si Tran[1], Christian Lüchtenborg[2], Philip V'kovski[3,4], Katrin Hörmann[5], André C. Müller[5], Carolin Zitzmann[6‼], Uta Haselmann[1], Jürgen Beneke[7], Lars Kaderali[6], Holger Erfle[7], Volker Thiel[3,4], Volker Lohmann[1], Giulio Superti-Furga[5,8], Britta Brügger[2], and Ralf Bartenschlager[1,9,10, &]

Affiliations:

[1]Department of Infectious Diseases, Molecular Virology, Heidelberg University, Heidelberg, Germany

[2]Biochemistry Center Heidelberg, Heidelberg University, Heidelberg, Germany

[3]Institute of Virology and Immunology IVI, Bern, Switzerland.

[4]Department of Infectious Diseases and Pathobiology, Vetsuisse Faculty, University of Bern, Bern, Switzerland.

[5]CeMM Research Center for Molecular Medicine of the Austrian Academy of Sciences, Vienna, Austria.

[6]Institute of Bioinformatics and Center for Functional Genomics of Microbes, University Medicine Greifswald, Greifswald, Germany.

[7]BioQuant, Heidelberg University, Heidelberg, Germany.

[8]Center for Physiology and Pharmacology, Medical University of Vienna, Vienna, Austria.

[9]Division Virus-Associated Carcinogenesis, German Cancer Research Center, Heidelberg, Germany

[10]German Center for Infection Research, Heidelberg Partner Site, Heidelberg, Germany

†Keisuke Tabata: Department of Genetics, Graduate School of Medicine, Osaka University, Osaka, Japan; Laboratory of Intracellular Membrane Dynamics, Graduate School of Frontier Biosciences, Osaka University

‡David Paul: MRC Laboratory of Molecular Biology, Francis Crick Avenue, Cambridge CB2 0QH, UK

‼Carolin Zitzmann: Los Alamos National Laboratory, Theoretical Biology and Biophysics Los Alamos, NM, USA

* These authors contributed equally to this work

& Correspondence:
Ralf Bartenschlager: ralf.bartenschlager@med.uni-heidelberg.de ; Phone: +49-6221-564225; Fax: +49-6221-564570

bioRxiv preprint doi: https://doi.org/10.1101/2021.05.10.443480; this version posted May 10, 2021. The copyright holder for this preprint (which was not certified by peer review) is the author/funder. All rights reserved. No reuse allowed without permission.

Abstract

Double membrane vesicles (DMVs) are used as replication organelles by phylogenetically and biologically distant pathogenic RNA viruses such as hepatitis C virus (HCV) and severe acute respiratory syndrome coronavirus-2 (SARS-CoV-2). Viral DMVs are morphologically analogous to DMVs formed during autophagy, and although the proteins required for DMV formation are extensively studied, the lipids driving their biogenesis are largely unknown. Here we show that production of the lipid phosphatidic acid (PA) by acylglycerolphosphate acyltransferase (AGPAT) 1 and 2 in the ER is important for DMV biogenesis in viral replication and autophagy. Using DMVs in HCV-replicating cells as model, we found that AGPATs are recruited to and critically contribute to HCV replication and DMV formation. AGPAT1/2 double knockout also impaired SARS-CoV-2 replication and the formation of autophagosome-like structures. By using correlative light and electron microscopy, we observed the relocalization of AGPAT proteins to HCV and SARS-CoV-2 induced DMVs. In addition, an intracellular PA sensor accumulated at viral DMV formation sites, consistent with elevated levels of PA in fractions of purified DMVs analyzed by lipidomics. Apart from AGPATs, PA is generated by alternative pathways via phosphotidylcholine (PC) and diacylglycerol (DAG). Pharmacological inhibition of these synthesis pathways also impaired HCV and SARS-CoV-2 replication as well as formation of autophagosome-like DMVs. These data identify PA as an important lipid used for replication organelle formation by HCV and SARS-CoV-2, two phylogenetically disparate viruses causing very different diseases, i.e. chronic liver disease and COVID-19, respectively. In addition, our data argue that host-targeting therapy aiming at PA synthesis pathways might be suitable to attenuate replication of these viruses.

One Sentence Summary

Phosphatidic acid is important for the formation of double membrane vesicles, serving as replication organelles of hepatitis C virus and SARS-CoV-2, and offering a possible host-targeting strategy to treat SARS-CoV-2 infection.

Main Text

Chronic hepatitis C and COVID-19 are major medical problems. Both diseases are caused by viral infections inflicting a large number of people and having led to millions of deaths [1, 2]. Chronic hepatitis C is caused by persistent infection with the hepatitis C virus (HCV), while COVID-19 is due to acute infection with the severe acute respiratory syndrome coronavirus-2 (SARS-CoV-2). Both viruses are biologically very distinct e.g. by having a very narrow tropism and a predominantly persistent course of infection in the case of HCV, contrasting the rather broad tropism and acute self-limiting course of infection in the case of SARS-CoV-2. This biological distinction is reflected by their phylogenetic distance with HCV belonging to the *Flaviviridae* and SARS-CoV-2 being a member of the *Coronaviridae* virus family [3]. In spite of these differences, both viruses possess a single strand RNA genome of positive polarity that is replicated in membranous vesicles in the cytoplasm of infected cells [4, 5]. These vesicles are induced by viral proteins, in concert with cellular factors, and composed of two membrane bilayers, thus corresponding to double-membrane vesicles (DMVs). These DMVs accumulate in infected cells and can be regarded as viral replication organelle. Viral DMVs have morphological similarity to autophagosomes [6, 7], but while autophagy-induced DMVs serve to engulf cellular content and damaged organelles for subsequent degradation, viral DMVs create a conducive and protective environment for productive viral RNA replication. In the case of HCV and SARS-CoV-2, DMVs are derived

bioRxiv preprint doi: https://doi.org/10.1101/2021.05.10.443480; this version posted May 10, 2021. The copyright holder for this preprint (which was not certified by peer review) is the author/funder. All rights reserved. No reuse allowed without permission.

from the ER [8, 9, 10] and can be induced by the nonstructural proteins (NS)3, 4A, 4B, 5A and 5B in the case of HCV [7] and the viral proteins nsp3-4 in the case of MERS-CoV and SARS-CoV [11, 12], alongside with co-opted host cell proteins and lipids. Here, we set-out to search for common host cell factors exploited by the phylogenetically distant HCV and SARS-CoV-2 to build up their cytoplasmic replication organelle.

Using HCV as a model to study DMV biogenesis, we purified DMVs under native conditions and determined their molecular composition by proteomic profiling (Fig. 1A and B). To this end we used human hepatoma cells (Huh7) containing a self-replicating HCV replicon RNA (designated sg4B^{HA}31R; [13]) in which NS4B was HA-tagged (fig. S1A). This RNA replicates autonomously and induces an extensive array of DMVs that can be isolated by HA-affinity purification [13]. Mass spectrometry-based proteomics analysis identified a total of 1487 proteins significantly enriched in the NS4B-HA sample relative to the untagged technical negative control (using SAINT average *P*-values >0.95) (data S1). Label free quantitation (LFQ) revealed a major overlap of proteins (1542) between the NS4B-HA complex and HCV-naïve ER membranes purified in parallel from Huh7 cells stably expressing HA-tagged Calnexin (CNX-HA) (Fig. 1B and fig. S1B). Of note, 309 proteins were significantly enriched in the NS4B-HA sample relative to the ER control with an over-representation of proteins involved in RNA metabolism, intracellular vesicle organization and transport as well as endomembrane organization (fig. S2). Given our interest in identifying proteins of relevance for DMV formation, we selected 139 candidates with a bias for proteins involved in vesicle transport and biogenesis as well as lipid metabolism. These candidates were validated with respect to their role in HCV replication by using RNA interference-based screening (Fig. 1C and data S2). In this way we could validate 38 hits as HCV dependency factors. Amongst identified hits were acylglycerolphosphate acyltransferase (AGPAT) 1 and 2, two enzymes that catalyze the *de novo* formation of phosphatidic acid (PA), a precursor to di- and triacylglycerols as well as all glycerophospholipids [14, 15]. In addition, PA is involved in signaling and protein recruitment to membranes and, owing to its small and highly charged head group, promotes membrane curvature [16, 17, 18]. Since these properties might be involved in DMV formation, we focused our subsequent analysis on AGPATs.

AGPATs play crucial roles in lipid homeostasis, because enzyme-inactivating mutations in AGPAT2 are linked to congenital generalized lipodystrophy and defects in PA metabolism as well as autophagy are associated with neurological disorders and chronic obstructive pulmonary disease [18, 19]. Moreover, severe lipodystrophy as well as extreme insulin resistance and hepatic steatosis have been observed in AGPAT2$^{-/-}$ mice [14]. To date, 11 AGPATs have been identified in mammalian cells. AGPAT1 to 5 preferentially utilize lysophosphatidic acid (LPA) as an acyl donor while AGPAT6 to 11 preferentially utilize alternative lysophospholipid substrates or have a preference for glycerol-3-phosphate. Thus, only AGPAT1 to 5 function as true LPA acyltransferases [14]. To establish which AGPAT family members are found in NS4B-associated membranes, FLAG-tagged versions of each of the 5 AGPATs were transiently expressed in cells containing the HCV replicon sg4B^{HA}31R (fig. S3A). Pull-down of NS4B-HA revealed association with AGPAT1 and 2, and to a lesser extent with AGPAT3, but not with AGPAT4 and 5. Additionally, endogenous AGPAT1 and 2 were detected in NS4B-HA containing membranes isolated from replicon-containing cells (Fig. 1D), whereas AGPAT 3 was not enriched. Moreover, in HCV infected cells AGPAT1 and 2 were recruited to NS4B-containing sites that most likely correspond to sites of DMV accumulation [13] (Fig. 1E).

To validate the role of AGPAT1 and 2 in HCV replication, we created knock-out cells using CRISPR/Cas9. Although we observed reduced cell growth of stable double knock-out (DKO) cells 8 days after transduction of guide RNAs, single KO cell pools showed no decrease in cell growth and could be used for transient knock-out of the other AGPAT gene without impacting cell viability for up to 8 days after transduction (fig. S3B). Using this approach, we observed that AGPAT1/2 DKO impaired lipid droplet formation (fig. S3, C to

bioRxiv preprint doi: https://doi.org/10.1101/2021.05.10.443480; this version posted May 10, 2021. The copyright holder for this preprint (which was not certified by peer review) is the author/funder. All rights reserved. No reuse allowed without permission.

E) as shown previously [20, 21], confirming disruption of AGPAT1/2 function. To monitor the impact of single KO and AGPAT1/2 DKO on HCV replication, cells were infected with an HCV reporter virus and viral replication was determined by using luciferase assay. While single KO suppressed HCV replication by ~50-70%, a reduction by ~90% was observed in DKO cells (Fig. 1F). Even stronger replication suppression was observed with a subgenomic replicon (fig. S4A), confirming that AGPAT depletion affected viral RNA replication and not virus entry or assembly. Of note, replication was completely restored by stable expression of AGPAT1 and 2 in DKO cells, which was not the case with either or both enzymatically inactive mutants (Fig. 1G). In contrast, replication of Dengue virus (DENV) and Zika virus (ZIKV), also belonging to the *Flaviviridae* family, but inducing morphologically different membrane alterations, i.e. ER membrane invaginations [4], was not affected as determined by plaque assay or with a reporter virus (Fig. 1H and fig. S4B, respectively). These results suggest that enzymatically active AGPAT1 and 2 are required for HCV replication with both AGPATs having partially redundant functions.

Next, we determined the impact of AGPAT KO on HCV-induced DMV formation. Since AGPAT1/2 DKO reduces RNA replication, we employed a replication-independent system in which DMV production is induced by the sole expression of an HCV NS3-5B polyprotein fragment that undergoes self-cleavage to produce functional NS3, 4A, 4B, 5A and 5B [8, 22] (Fig. 2A). To determine the replicase subcellular location by fluorescence microscopy, NS5A was fluorescently tagged with EGFP. This tagging has no effect on replicase functionality [8, 22]. While expression of this polyprotein induced a high number of DMVs in control cells, DMV abundance was dramatically reduced in AGPAT1/2 DKO cells (Fig. 2, A and B), although amounts of viral proteins were comparable in control and DKO cell pools (Fig. 2C). Moreover, DMVs had a smaller diameter in AGPAT2 KO cells (fig. S4C). These results argue for a pivotal role of AGPATs in HCV DMV biogenesis.

Given that AGPAT1 and 2 are important for DMV formation and their enzymatic activity is required for HCV replication, we next focused on their reaction product, i.e. the lipid PA. To quantify the amount of PA associated with HCV-induced DMVs and compare it to ER membranes, we determined the lipidome of highly purified DMVs isolated from cells containing the sg4B^{HA}31R replicon (Fig. 2D). Consistent with earlier results, these membranes contained elevated amounts of cholesterol and sphingolipids, which served as positive controls, relative to ER membranes purified in parallel [13, 23]. Of note, PA abundance in DMVs also was increased in comparison to ER membranes, whereas the level of diacyl phosphatidylcholine (aPC) and several other lipids was not affected (Fig. 2D; for further lipids see data S3).

To confirm these findings in single cells, we used two alternative methods to detect PA by fluorescence microscopy. First, we generated a recombinant protein composed of GST that was fused to the PA binding domain (PABD) derived from yeast Spo20p (fig. S5A and B). As a specificity control we employed the analogous sensor protein containing a mutation in the PABD that abolishes PA binding, and GST alone [24]. These proteins were introduced via transient permeabilization into Huh7 derived cells (fig. S5C). In cells treated with phorbol 12-myristate 13-acetate (PMA), a potent activator of phospholipase D-mediated PA production, as expected the intact sensor predominantly stained the plasma membrane, which was not the case with the PA non-binding mutant or GST alone, confirming specificity of the signal (fig. S5D). Moreover, also in cells that were not treated with PMA, the PA sensor predominantly stained the plasma membrane (fig. S5D, right panel). Using this assay, we monitored intracellular PA distribution in HCV replicon-containing cells and observed PA colocalization with NS4B (fig. S5E). As second assay for intracellular PA detection, we created a GFP-tagged sensor fused to the PABD of Raf1, a serine-threonine kinase recruited to cellular membranes via its interaction with Ras and PA [25]. While in control Huh7 cells this PA sensor displayed a diffuse pattern (fig. S6A), upon co-expression of the HCV NS3-5B polyprotein the sensor accumulated in NS5A-positive puncta (Fig. 2E). Of note, a control PA

bioRxiv preprint doi: https://doi.org/10.1101/2021.05.10.443480; this version posted May 10, 2021. The copyright holder for this preprint (which was not certified by peer review) is the author/funder. All rights reserved. No reuse allowed without permission.

sensor containing mutations in the PABD of Raf1 (mutant 4E) [26] displayed only a diffuse pattern in NS3-5B expressing cells (Fig. 2E), supporting specificity of the signal and PA recruitment to HCV replication sites.

Since these data suggest an important role of AGPAT1 and 2-dependent PA enrichment on HCV-induced DMVs, we hypothesized that other pathways contributing to PA generation in cells might also play a role in HCV replication. Apart from AGPATs, one other route for PA synthesis is through hydrolysis of phosphatidylcholine (PC) by phospholipase D1 (PLD1) and D2 (PLD2) enzymes (Fig. 2F, top panel) [17, 27]. To test the role of PLD1/2 enzymes in HCV replication, we employed a pharmacological approach using 3 different PLD1/2 inhibitors. Treatment with PLD2 inhibitor ML298 caused replication inhibition at a concentration that did not significantly reduce cell viability (~25 μM; Fig. 2F, bottom panel), whereas for the other drugs the reduction in HCV replication correlated with cytotoxicity (not shown). In summary, these results suggest that PA generated via AGPAT1/2, and possibly by alternative PA synthesis pathway, contributes to HCV replication by supporting the formation of DMVs, which is the site of viral RNA amplification.

Virus-induced DMVs are morphologically analogous to autophagosomes generated during autophagy [7]; therefore, we tested if PA would be recruited to and is required for autophagy-induced DMVs. To this end, we monitored the localization of the GFP tagged PA sensor with markers for DMVs induced during nonselective and selective autophagy. To monitor DMV formation induced during nonselective autophagy, cells were incubated in starvation medium with or without bafilomycin A1 (BafA1), an inhibitor of the vacuolar-type H^+-ATPase inducing the accumulation of LC3-positive puncta, which are indicative of autophagosomes. For selective autophagy events, we focused on the induction of DMVs during mitophagy induced by treatment of the cells with valinomycin (Val) [28, 29]. As shown in Fig. 2G (top row), the PA sensor GFP-PABD-Raf1 was rather uniformly distributed throughout the cell in non-induced cells. However, induction of nonselective autophagy by serum starvation led to a significant increase in the number of LC3 puncta with GFP-PABD-Raf1 relocalizing to these puncta (Fig. 2G). Similarly, induction of mitophagy by Val treatment caused an abundant association of mCherry-Parkin puncta with GFP-PABD-Raf1 (Fig. 2G, lower panel), whereas in control cells not treated with Val, no such association was found (fig. S6B). Next, we investigated the functional role of PA generation during nonselective and selective autophagy. Consistent with the relocalization of PA to LC3 puncta during nonselective autophagy, PA inhibitors targeting PLD1, PLD2 and AGPATs, applied as short-term treatments and at non-toxic concentrations, significantly reduced the accumulation of LC3 puncta (fig. S7). These findings are consistent with a recent study suggesting that PA generated on the ATG16L1-positive autophagosome precursor membrane contributes to autophagosome formation [30]. Of note, a third pathway for PA production via phosphorylation of diacylglycerol (DAG) by diacylglycerol kinase (DAGK) [27], did not contribute to PA accumulation or increase in LC3 puncta during nonselective autophagy (fig. S7).

Having found that AGPAT1 and 2, and their reaction product PA, are involved in DMV formation induced upon HCV infection and in, morphologically similar, DMVs generated during autophagy, we hypothesized that AGPATs and PA might also be involved in the biogenesis of replication organelles of other unrelated RNA viruses, e.g., coronaviruses, which also utilize DMVs as viral replication sites [9, 10]. Hence, we investigated the role of AGPATs in the DMV biogenesis of SARS-CoV-2, the causative agent of the ongoing COVID-19 pandemic. In the first set of experiments, we studied the recruitment of AGPATs to SARS-CoV-2 induced DMVs. In the case of MERS-CoV and SARS-CoV, formation of DMVs with structural resemblance to those observed in infected cells can be induced by the sole expression of viral nonstructural protein (nsp)3-4, which is an ~270 kilodalton large polyprotein fragment undergoing self-cleavage [12]. Building on these results we first determined whether the same applies to SARS-CoV-2. Huh7-derived cells stably expressing

bioRxiv preprint doi: https://doi.org/10.1101/2021.05.10.443480; this version posted May 10, 2021. The copyright holder for this preprint (which was not certified by peer review) is the author/funder. All rights reserved. No reuse allowed without permission.

T7 RNA polymerase were transiently transfected with a T7 promoter driven SARS-CoV-2 HA-nsp3-4-V5 expression construct or the empty vector (fig S8A). Using immunofluoresence with an HA-specific antibody in many cells we observed clusters of HA-nsp3 (fig. S8B). Western blotting confirmed efficient self-cleavage between nsp3 and nsp4 (fig. S8C). To identify membrane alterations in HA-nsp3-4-V5 expressing cells, we employed CLEM. Cells were transfected with the analogous expression construct encoding in addition the NeonGreen gene to allow visualization of transfected cells by fluorescence microscopy (fig. S8D). NeonGreen positive cells were recorded and examined by transmission electron microscopy, revealing abundant clusters of DMVs (fig S8D). Comparison of DMVs induced by nsp3-4 expression and by SARS-CoV-2 infection revealed similar morphology, although expression-induced DMVs were smaller (~125 nm compared to ~300 nm, respectively) (fig S8E). These results show that the sole expression of SARS-CoV-2 nsp3-4 is sufficient to induce DMVs with structural similarity to those generated in infected cells.

Next, we employed this expression-based system to determine AGPAT function in SARS-CoV-2 nsp3-4 induced DMV formation. Huh7-derived cells expressing GFP-tagged AGPAT1 or 2 were transiently transfected with the SARS-CoV-2 HA-nsp3-4-V5 encoding plasmid or the empty vector and colocalization of AGPATs with HA-nsp3 was determined by immunofluorescence microscopy. While in empty vector-transfected cells AGPAT2 and 1 were homogeneously distributed throughout the ER (Fig. 3A and fig. S9A, respectively), we observed a strong relocalization of AGPATs in HA-nsp3-4-V5 expressing cells with AGPATs forming puncta that colocalized with HA-nsp3 (Fig. 3, A and B; fig. S9A). Of note, the relocalization of AGPATs induced by HA-nsp3-4-V5 was not the result of the massive ER alterations occurring in SARS-CoV-2 infected cells, since the subcellular distribution of other ER resident proteins, such as protein disulfide-isomerase (PDI) and calnexin remained unaffected compared to the large puncta observed with AGPATs (Fig. 3C). Since SARS-CoV-2 replication organelles are comprised of DMVs, convoluted membranes and zippered ER [31], we next investigated the membrane structures at the sites of AGPAT colocalization with HA-nsp3-4-V5. Using correlative light electron microscopy, we found that relocalized AGPAT puncta perfectly correlated with extensive networks of SARS-CoV-2 HA-nsp3-4-V5 induced DMVs (Fig. 3D). Overall, the data shown here suggest that similar to HCV, AGPATs are relocalized to SARS-CoV-2 nsp3-4 induced DMVs, the likely sites of viral RNA replication [32].

Next, we tested the effect of AGPAT1/2 depletion on SARS-CoV-2 infection and replication. To this end we used DKO Huh7-Lunet/T7 cells that were employed for the imaging analyses described so far and stably introduced the SARS-CoV-2 receptor gene *ACE2*. Viral replication was measured by using an image-based assay that quantifies the number of cells containing detectable amounts of the nucleocapsid (N) protein (fig. S9B). Using this approach, we observed significant reduction of SARS-CoV-2 positive cells in both single and double AGPAT knockout cells (Fig. 3E). Consistently, RT-qPCR revealed similar reduction of viral replication in single and double KO cells (Fig. 3E, lower right panel). To determine if reduced SARS-CoV-2 replication in AGPAT1/2 KO cells might correlate with altered DMV formation, we transiently expressed SARS-CoV-2 HA-nsp3-4-V5 in control, single and double KO cells. The absence of AGPAT 1/2 did not significantly affect the abundance of cleaved viral proteins HA-nsp3 and nsp4-V5 (fig. S8C). EM analysis of control cells revealed HA-nsp3-4-V5 induced membrane alterations, consistent with an earlier report for MERS-CoV and SARS-CoV [12] (Fig. 3, F and G). This included zippered ER and DMVs with an average diameter of 145 nm. In contrast to HCV, the number of nsp3-4 induced DMVs did not decrease in AGPAT single and double KO cells (Fig. 3G, left two panels). However, in both cell pools we observed marked accumulations of multi-membrane vesicles (MMVs), indicating the formation of aberrant membrane structures (Fig. 3, F and G).

bioRxiv preprint doi: https://doi.org/10.1101/2021.05.10.443480; this version posted May 10, 2021. The copyright holder for this preprint (which was not certified by peer review) is the author/funder. All rights reserved. No reuse allowed without permission.

To test whether similar to AGPAT1/2 relocalization to nsp3-4 induced DMVs, PA is also enriched at those sites we used the GFP-tagged PA sensor derived from Raf1. In Huh7-derived cells expressing SARS-CoV-2 HA-nsp3-4-V5, the functional version of the sensor (GFP-PABD-Raf1-WT) strongly colocalized with HA-nsp3 in distinct puncta, whereas no such puncta were found with the mutant PABD-Raf1, confirming specificity of PA sensor recruitment to HA-nsp3-containing sites (Fig. 4, A and B).

Although in comparison to HCV, AGPAT1/2 DKO had lower impact on SARS-CoV-2 replication (compare Fig. 1F with Fig. 3E), and caused a morphologically distinct phenotype of nsp3-4 induced DMVs (Fig. 2A and 3F, respectively), AGPATs, and most likely PA, still accumulated at sites of SARS-CoV-2 DMV clusters (Fig. 4, A and B). This indicates that PA synthesis pathways other than via AGPAT1/2, might contribute to SARS-CoV-2 replication and DMV formation. By means of pharmacological inhibitors of enzymes that convert LPA, PC and DAG to PA (fig. S7A), we measured the dose-dependent effect of these drugs on SARS-CoV-2 replication. All inhibitors reduced SARS-CoV-2 replication in Calu-3 cells and in A549 cells stably expressing ACE2, two commonly used cell models for this virus, at non-cytotoxic concentrations, although in the case of the general AGPAT inhibitor CI976 selectivity was rather low (Fig. 4C and fig. S10A, respectively). Of note, combining the inhibitors at concentrations close to or below their IC50 values caused much stronger reduction of virus replication with no or minimal effect on cell viability, indicating that SARS-CoV-2 can utilize PA produced by alternative PA synthesis pathways (fig. S10, A and B). We then measured the effect of these drugs on PA accumulation at HA-nsp3 containing puncta in HA-nsp3-4-V5 expressing cells and found that all inhibitors reduced PA levels at these sites (Fig. 4D). This reduction was not the result of altered HA-nsp3-4-V5 expression level or self-cleavage, which were unaffected in inhibitor-treated cells (fig. S10C). Next, we determined if reduced PA levels caused by these inhibitors also affect SARS-CoV-2 nsp3-4 induced DMV formation. In cells treated with AGPAT, PLD1, and DAGK inhibitors DMV diameters were significantly reduced (Fig. 4, E and F). Moreover, PLD2 inhibition promoted the formation of MMVs and larger DMVs, similar to what we found in AGPAT single and double KO cells (Fig. 3F). Taken together, our data suggest that PA enrichment is important for proper SARS-CoV-2 DMV formation and viral replication.

Here, we show that PA produced by AGPAT1 and 2 is important for the replication of evolutionary distant positive-strand RNA viruses, HCV and SARS-CoV-2 that amplify their genome in association with DMVs. The remarkable dependence on a common host lipid for the DMV biogenesis in these two viruses that differ profoundly in the diseases they cause and in their biological properties, indicates a striking similarity in the biogenesis of these organelles. Conversely, for viruses replicating their RNA genome in ER-derived membrane invaginations such as the flaviviruses DENV and ZIKV, this lipid pathway appears to be dispensable [4, 33]. Of note, PA production through AGPAT1 and 2 is also involved in the formation of autophagosome-like DMVs, arguing for some similarity between cellular and viral DMV formation and lipid composition. Additionally, alternative routes of PA biosynthesis contribute to HCV and SARS-CoV-2 replication and DMV generation.

At least three possibilities can be envisioned how PA promotes DMV formation in viral replication and in the context of autophagy. First, the presence of lipids with cone or inverted cone shape in membranes contributes to membrane bending by generating negative or positive membrane curvature, respectively [16]. While LPA has a large polar head group to fatty acid tail ratio, giving rise to an inverse-cone shape and resulting in positive membrane curvature, the additional fatty acid tail present in PA inverses the head-to-tail ratio. Hence PA displays an overall cone shape, which contributes to negative membrane curvature. Thus, the LPA - PA conversion by AGPATs might contribute to DMV formation by facilitating membrane curvature. Second, PA is directly or indirectly implicated in membrane fission [34]. This might be achieved by recruitment of effector proteins by PA, either through downstream signaling events, or directly by serving as docking site for PA-binding proteins that have

bioRxiv preprint doi: https://doi.org/10.1101/2021.05.10.443480; this version posted May 10, 2021. The copyright holder for this preprint (which was not certified by peer review) is the author/funder. All rights reserved. No reuse allowed without permission.

amphipathic or hydrophobic surfaces. In this regard, our NS4B-proteome showed the enrichment of three known PA-interacting proteins, namely, Vitronectin, splicing factor-1, and ubiquitin carboxy-terminal hydrolase L1, in the viral DMV fraction (data S1) [35]. More than 50 different proteins have been reported to interact with PA, including protein kinases, phosphatases, nucleotide-binding proteins and regulators, however, a comprehensive list remains elusive, and their possible role in the formation of DMVs during autophagy or viral RNA replication, if any, remains to be determined [18]. Third, an additional role of PA for the functionality of viral replication organelles and perhaps also autophagosomes might be in serving as an exchange lipid in a counter-transporter chain. In the case of HCV, we and others identified accumulation of PI4P at DMVs [7] and similar findings have been made for membranous structures involved in the early steps of autophagy [36]. For HCV, it is thought that PI4P recruits lipid transporters such as OSBP that deliver cholesterol into DMV membranes in exchange for PI4P. A similar mechanism might apply for other lipids or the PI4P precursor PI, with PA serving as a possible exchange factor against these other lipids or PI, respectively.

The similar dependency of DMV-type replication organelles on PA, as reported here for HCV and SARS-CoV-2, might offer an attractive starting point for broad-spectrum antivirals targeting a diverse range of positive-strand RNA viruses replicating in such structures. In line with this assumption, an inhibitor of cytosolic phospholipase $A_2\alpha$ has been reported to suppress replication and DMV formation of the 229E human coronavirus and to exert antiviral activity also against the alphavirus Semliki forest virus [37]. In addition, several human diseases have been linked to defects in PA metabolism and selective autophagy, including neurological disorders and chronic obstructive pulmonary disease [18, 19]. Although the precise role of PA in these diseases remains to be determined, the critical role of PA for HCV and SARS-CoV-2 infection reported here might offer new approaches for therapeutic intervention.

References and Notes:

1. W H O Situation Reports. Coronavirus disease (COVID-19) Weekly Epidemiological Update and Weekly Operational Update.) (2021).

2. Spearman CW, Dusheiko GM, Hellard M, Sonderup M. Hepatitis C. *Lancet* **394**, 1451-1466 (2019).

3. Wolf YI*, et al.* Origins and Evolution of the Global RNA Virome. *mBio* **9**, (2018).

4. Neufeldt CJ, Cortese M, Acosta EG, Bartenschlager R. Rewiring cellular networks by members of the Flaviviridae family. *Nat Rev Microbiol* **16**, 125-142 (2018).

5. V'Kovski P, Kratzel A, Steiner S, Stalder H, Thiel V. Coronavirus biology and replication: implications for SARS-CoV-2. *Nat Rev Microbiol* **19**, 155-170 (2021).

6. Lamb CA, Yoshimori T, Tooze SA. The autophagosome: origins unknown, biogenesis complex. *Nat Rev Mol Cell Biol* **14**, 759-774 (2013).

7. Paul D, Bartenschlager R. Flaviviridae Replication Organelles: Oh, What a Tangled Web We Weave. *Annu Rev Virol* **2**, 289-310 (2015).

bioRxiv preprint doi: https://doi.org/10.1101/2021.05.10.443480; this version posted May 10, 2021. The copyright holder for this preprint (which was not certified by peer review) is the author/funder. All rights reserved. No reuse allowed without permission.

8. Romero-Brey I, *et al.* Three-dimensional architecture and biogenesis of membrane structures associated with hepatitis C virus replication. *PLoS Pathog* **8**, e1003056 (2012).

9. Cortese M, *et al.* Integrative Imaging Reveals SARS-CoV-2-Induced Reshaping of Subcellular Morphologies. *Cell Host Microbe* **28**, 853-866 e855 (2020).

10. Snijder EJ, *et al.* A unifying structural and functional model of the coronavirus replication organelle: Tracking down RNA synthesis. *PLoS biology* **18**, e3000715 (2020).

11. Wolff G, Melia CE, Snijder EJ, Barcena M. Double-Membrane Vesicles as Platforms for Viral Replication. *Trends Microbiol* **28**, 1022-1033 (2020).

12. Oudshoorn D, *et al.* Expression and Cleavage of Middle East Respiratory Syndrome Coronavirus nsp3-4 Polyprotein Induce the Formation of Double-Membrane Vesicles That Mimic Those Associated with Coronaviral RNA Replication. *mBio* **8**, (2017).

13. Paul D, Hoppe S, Saher G, Krijnse-Locker J, Bartenschlager R. Morphological and biochemical characterization of the membranous hepatitis C virus replication compartment. *J Virol* **87**, 10612-10627 (2013).

14. Yamashita A, *et al.* Glycerophosphate/Acylglycerophosphate acyltransferases. *Biology (Basel)* **3**, 801-830 (2014).

15. Takeuchi K, Reue K. Biochemistry, physiology, and genetics of GPAT, AGPAT, and lipin enzymes in triglyceride synthesis. *Am J Physiol Endocrinol Metab* **296**, E1195-1209 (2009).

16. Kooijman EE, Chupin V, de Kruijff B, Burger KN. Modulation of membrane curvature by phosphatidic acid and lysophosphatidic acid. *Traffic* **4**, 162-174 (2003).

17. Zegarlinska J, Piascik M, Sikorski AF, Czogalla A. Phosphatidic acid - a simple phospholipid with multiple faces. *Acta Biochim Pol* **65**, 163-171 (2018).

18. Tanguy E, Wang Q, Moine H, Vitale N. Phosphatidic Acid: From Pleiotropic Functions to Neuronal Pathology. *Front Cell Neurosci* **13**, 2 (2019).

19. Mizumura K, Choi AM, Ryter SW. Emerging role of selective autophagy in human diseases. *Front Pharmacol* **5**, 244 (2014).

bioRxiv preprint doi: https://doi.org/10.1101/2021.05.10.443480; this version posted May 10, 2021. The copyright holder for this preprint (which was not certified by peer review) is the author/funder. All rights reserved. No reuse allowed without permission.

20. Fernandez-Galilea M, Tapia P, Cautivo K, Morselli E, Cortes VA. AGPAT2 deficiency impairs adipogenic differentiation in primary cultured preadipocytes in a non-autophagy or apoptosis dependent mechanism. *Biochem Biophys Res Commun* **467**, 39-45 (2015).

21. Cautivo KM*, et al.* AGPAT2 is essential for postnatal development and maintenance of white and brown adipose tissue. *Mol Metab* **5**, 491-505 (2016).

22. Lee JY*, et al.* Spatiotemporal Coupling of the Hepatitis C Virus Replication Cycle by Creating a Lipid Droplet- Proximal Membranous Replication Compartment. *Cell Rep* **27**, 3602-3617 e3605 (2019).

23. Khan I*, et al.* Modulation of hepatitis C virus genome replication by glycosphingolipids and four-phosphate adaptor protein 2. *J Virol* **88**, 12276-12295 (2014).

24. Zhang F*, et al.* Temporal production of the signaling lipid phosphatidic acid by phospholipase D2 determines the output of extracellular signal-regulated kinase signaling in cancer cells. *Mol Cell Biol* **34**, 84-95 (2014).

25. Rizzo MA, Shome K, Watkins SC, Romero G. The recruitment of Raf-1 to membranes is mediated by direct interaction with phosphatidic acid and is independent of association with Ras. *J Biol Chem* **275**, 23911-23918 (2000).

26. Prakash P, Hancock JF, Gorfe AA. Three distinct regions of cRaf kinase domain interact with membrane. *Sci Rep* **9**, 2057 (2019).

27. Sakane F, Hoshino F, Murakami C. New Era of Diacylglycerol Kinase, Phosphatidic Acid and Phosphatidic Acid-Binding Protein. *Int J Mol Sci* **21**, (2020).

28. Yamano K*, et al.* Endosomal Rab cycles regulate Parkin-mediated mitophagy. *Elife* **7**, (2018).

29. Vargas JNS*, et al.* Spatiotemporal Control of ULK1 Activation by NDP52 and TBK1 during Selective Autophagy. *Mol Cell* **74**, 347-362 e346 (2019).

30. Holland P*, et al.* HS1BP3 negatively regulates autophagy by modulation of phosphatidic acid levels. *Nat Commun* **7**, 13889 (2016).

31. Knoops K*, et al.* SARS-coronavirus replication is supported by a reticulovesicular network of modified endoplasmic reticulum. *PLoS Biol* **6**, e226 (2008).

bioRxiv preprint doi: https://doi.org/10.1101/2021.05.10.443480; this version posted May 10, 2021. The copyright holder for this preprint (which was not certified by peer review) is the author/funder. All rights reserved. No reuse allowed without permission.

32. Wolff G*, et al.* A molecular pore spans the double membrane of the coronavirus replication organelle. *Science*, (2020).

33. Welsch S*, et al.* Composition and three-dimensional architecture of the dengue virus replication and assembly sites. *Cell Host Microbe* **5**, 365-375 (2009).

34. Pagliuso A*, et al.* Golgi membrane fission requires the CtBP1-S/BARS-induced activation of lysophosphatidic acid acyltransferase delta. *Nat Commun* **7**, 12148 (2016).

35. Jang J-H, Lee CS, Hwang D, Ryu SH. Understanding of the roles of phospholipase D and phosphatidic acid through their binding partners. In: *Prog. Lipid Res.*) (2012).

36. Judith D, Jefferies HBJ, Boeing S, Frith D, Snijders AP, Tooze SA. ATG9A shapes the forming autophagosome through Arfaptin 2 and phosphatidylinositol 4-kinase IIIbeta. *J Cell Biol* **218**, 1634-1652 (2019).

37. Muller C, Hardt M, Schwudke D, Neuman BW, Pleschka S, Ziebuhr J. Inhibition of Cytosolic Phospholipase A2alpha Impairs an Early Step of Coronavirus Replication in Cell Culture. *J Virol* **92**, (2018).

Acknowledgements

We thank Marie Bartenschlager, Lena Werstein, Ulrike Herian, Stephanie Kallis, Iris Leibrecht and Fredy Huschmand for excellent technical assistance. We are grateful to Eliana Acosta and Heeyoung Kim for editorial assistance. We acknowledge Alessia Ruggieri for providing empty plasmid constructs. We also acknowledge the excellent support provided by the Infectious Diseases Imaging Platform (IDIP) headed by Vibor Laketa, the University of Heidelberg Electron Microscopy Core Facility (EMCF Heidelberg) headed by Stefan Hillmer and the Proteomics and Metabolomics Facility (Pro-Met-) at CeMM. We thank the European Virus Archive (EVAg) for the provision of the HP/F/2013 ZIKV strain. We also thank all members of the Molecular Virology unit for continuous stimulating discussions.

Funding

This work was supported by grants from the Deutsche Forschungsgemeinschaft (DFG, German Research Foundation) – Project Number 272983813 – TRR 179, Project Number 112927078 - TRR 83 and Project Number 314905040 – TRR 209, all to R.B. and Project Number 112927078 - TRR 83, Project Number 240245660 - SFB1129, and Project Number 316659730 to B.B. V.P. is supported by a European Molecular Biology Organization (EMBO) Long-Term Fellowship (ALTF 454-2020). C.J.N was supported in part by a European Molecular Biology Organization (EMBO) Long-Term Fellowship (ALTF 466-2016). L.K. and C.Z. acknowledge funding from the BMBF, grant number 031A602A (ERASysApp SysVirDrug). P.V. and V.T. were supported by the Swiss National Science foundation (SNF Project Number 310030_173085). G. S.-F. and K. H. were supported by a European Research Council Advanced Investigator Grant (ERC AdG 695214 i-FIVE).

bioRxiv preprint doi: https://doi.org/10.1101/2021.05.10.443480; this version posted May 10, 2021. The copyright holder for this preprint (which was not certified by peer review) is the author/funder. All rights reserved. No reuse allowed without permission.

Contributions

Conceptualization, K.T., V.P., D.P., and R.B.; Investigation, K.T., V.P., D.P., J-Y.L., M-T.P., W-I.T, C.J.N., M.C., B.C., C-S.T., C.L., P.V., K.H., A.C.M, C.Z., U.H., J.B., L.K., B.B.; Writing – Original Draft, K.T., V.P., and R.B.; Writing – Review & Editing, K.T.,V.P., D.P., J.Y.L., C.J.N., A.M, A.C.M., L.K., H.E., V.T., G.S-F., B.B. and R.B.; Funding Acquisition, R.B., B.B., L.K. and G.S.-F.

Competing interests

Authors declare no competing interests.

Data and materials availability

All data is available in the main text or the supplementary materials.

Supplementary Materials:

Materials and Methods

Figures S1-S10

Tables S1-S5

References (*1-30*)

Other Supplementary Materials (Data S1-S3)

bioRxiv preprint doi: https://doi.org/10.1101/2021.05.10.443480; this version posted May 10, 2021. The copyright holder for this preprint (which was not certified by peer review) is the author/funder. All rights reserved. No reuse allowed without permission.

Figures

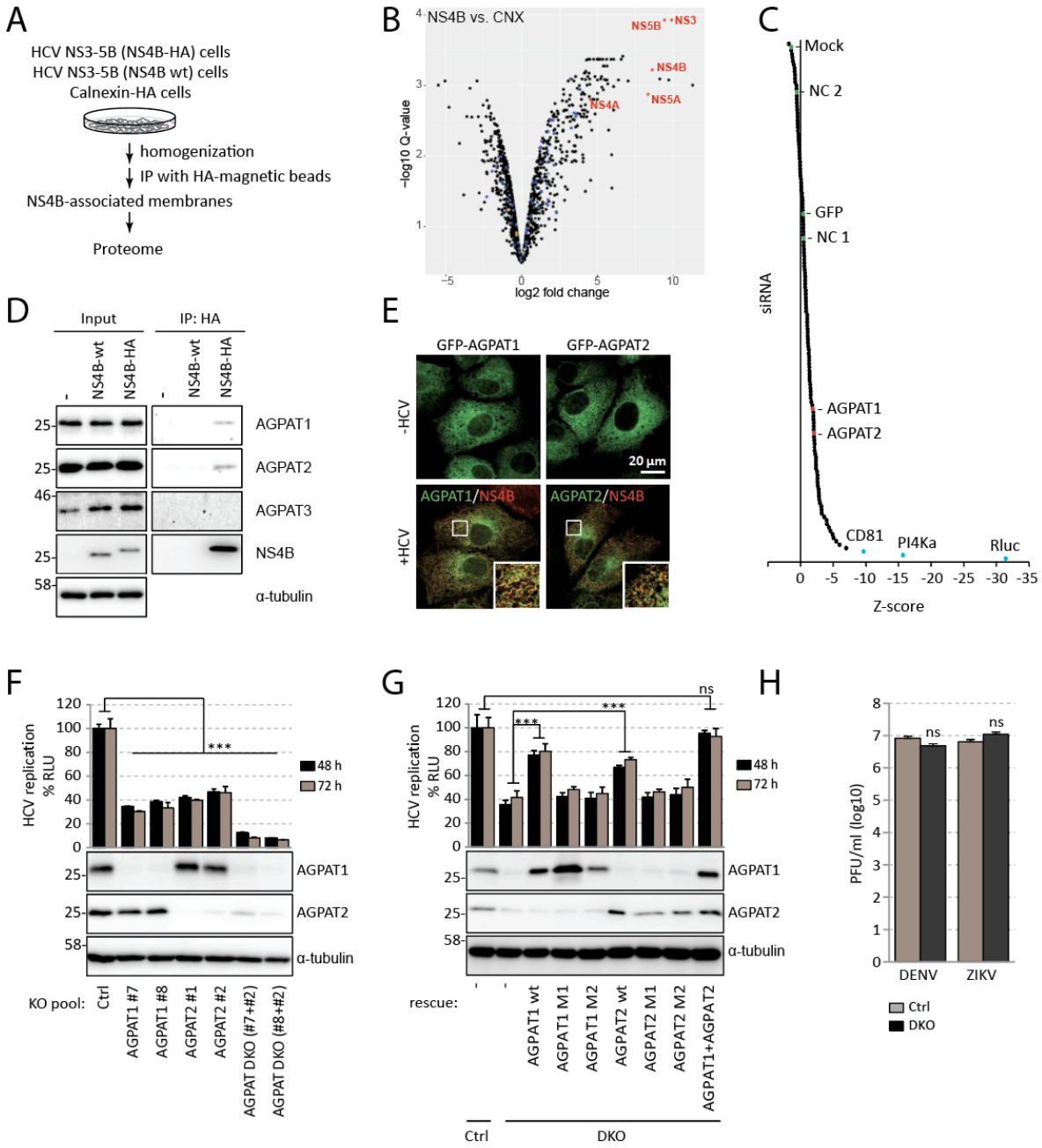

Fig. 1. Proteome analysis of HCV-induced DMVs identifies AGPATs as host dependency factors critically contributing to viral replication.
(**A**) Experimental approach used to purify DMVs from HCV-replicating cells. (**B**) Volcano plot of differentially enriched interactors of NS4B and calnexin (CNX). Q-values were calculated using the limma software package and corrected for multiple hypothesis testing. Viral proteins are highlighted with red letters. A magnified view with protein hits labeled is given in fig. S1B. (**C**) A total of 139 genes were selected from the DMV proteome and validated by siRNA screening (3 siRNAs per gene). CD81, PI4KA and Rluc were used as positive controls; NC (negative control)1, NC2, GFP and mock infection served as negative controls. A summary of the screening is given in Data S2. (**D**) Endogenous AGPAT1 and 2, but not AGPAT3 are contained in NS4B-associated membranes. Membranes were purified

bioRxiv preprint doi: https://doi.org/10.1101/2021.05.10.443480; this version posted May 10, 2021. The copyright holder for this preprint (which was not certified by peer review) is the author/funder. All rights reserved. No reuse allowed without permission.

from naïve Huh7-Lunet cells (-), or Huh7-Lunet cells containing a subgenomic replicon without or with an HA-tag in NS4B (NS4B-wt and NS4B-HA, respectively). Captured proteins were analyzed by western blot, along with the input (2%). α-tubulin served as loading control. (**E**) Colocalization of NS4B with AGPAT1 and 2. Huh7-Lunet cells stably expressing AGPAT1- or AGPAT2-GFP were transfected with *in vitro* transcripts of the HCV genome Jc1 and fixed 48 h post-transfection. (**F**) Effect of AGPAT KO on HCV replication. Huh7.5 cells were infected with lentiviruses encoding AGPAT-targeting-sgRNA and 5 days later, infected with an HCV reporter virus (JcR2a). After 48 h and 72 h, *renilla* luciferase activities in cell lysates, reflecting viral RNA replication, were quantified. Graph shows average and SD from 3 independent experiments. Significance was calculated by a paired t-test. ***, $p<0.001$. Abundance of AGPAT proteins is shown on the bottom. α-tubulin served as loading control. (**G**) Enzymatic activity of AGPAT is required for HCV replication. KO cells were reconstituted with sgRNA-resistant AGPAT wild-type (wt) or catalytically dead mutants (M1 and M2) by lentiviral transduction. Cells were infected with JcR2a, and *renilla* luciferase activities were quantified. Graph shows average and SD from 3 independent experiments. Significance was calculated by paired t-test. ***, $p<0.001$. ns, $p>0.05$. Note the complete rescue by AGPAT1 and 2 co-expression. Abundance of AGPAT proteins is shown below the graph; α-tubulin served as loading control. (**H**) AGPAT1/2 DKO does not affect DENV or ZIKV propagation. Cells were infected with DENV-2 (strain 16681) or ZIKV (strain H/PF/2013) and 48 h later virus titer was quantified by plaque assay. Graph shows the average and SD from 3 independent experiments. Significance was analyzed by a paired t-test. ns, $p>0.05$. PFU, plaque forming units.

bioRxiv preprint doi: https://doi.org/10.1101/2021.05.10.443480; this version posted May 10, 2021. The copyright holder for this preprint (which was not certified by peer review) is the author/funder. All rights reserved. No reuse allowed without permission.

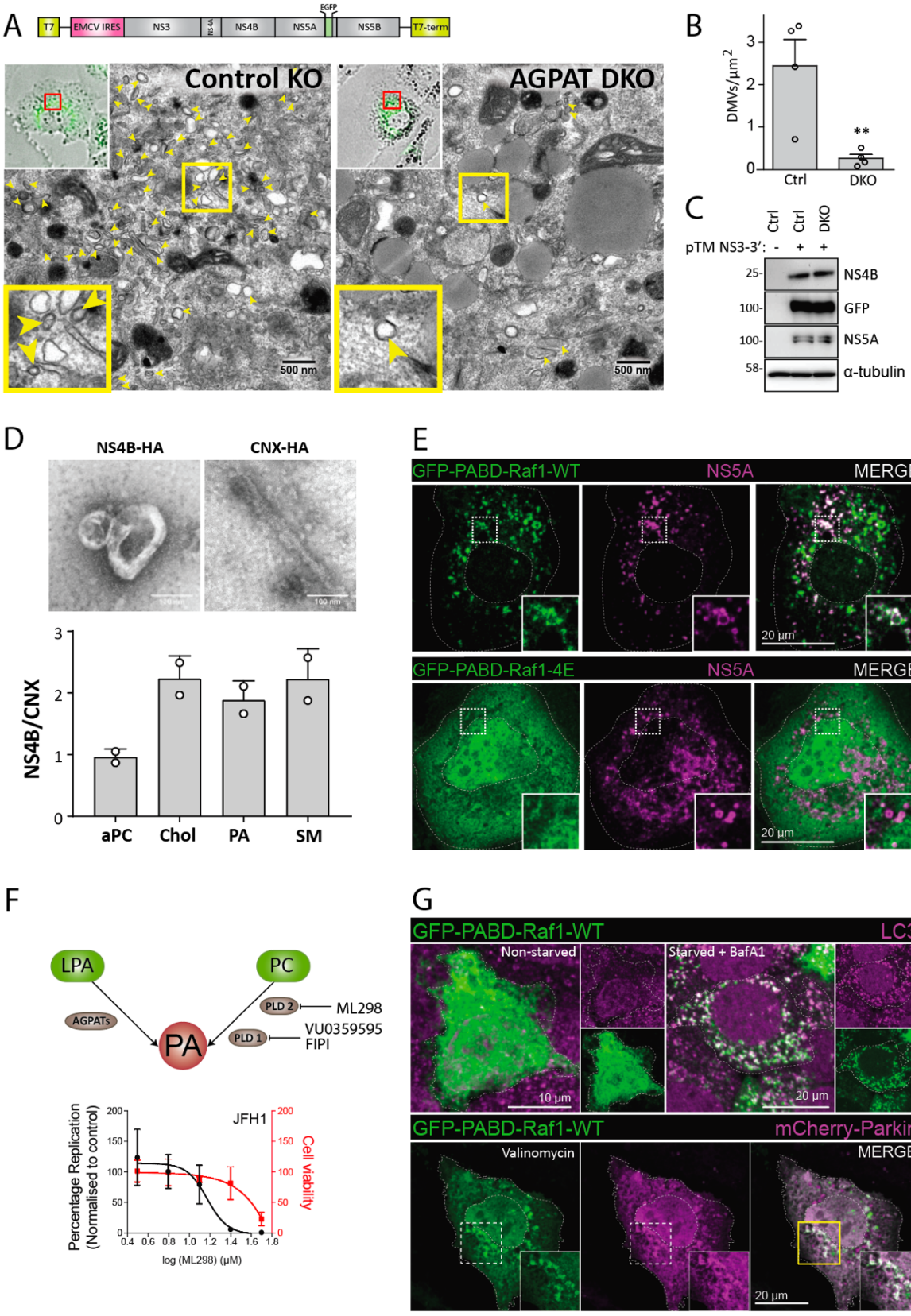

Fig. 2. Requirement of AGPATAs for HCV-induced DMV formation and PA accumulation on HCV-induced DMVs and autophagy-related structures.

(**A** to **C**) AGPAT1/2 DKO dampens DMV formation induced by HCV. Huh7-derived cells stably expressing the T7 RNA polymerase and containing or not a double knock-out (DKO)

bioRxiv preprint doi: https://doi.org/10.1101/2021.05.10.443480; this version posted May 10, 2021. The copyright holder for this preprint (which was not certified by peer review) is the author/funder. All rights reserved. No reuse allowed without permission.

of AGPAT1 and 2 were transfected with a HCV replicase-encoding plasmid containing a GFP insertion in NS5A (construct pTM NS3-3'/5A-GFP, top panel). Transcripts are generated from the plasmid in the cytoplasm via the T7 promoter and terminator (T7-term) sequence and the HCV NS3 – 5B coding region is translated via the IRES of the encephalomyocarditis virus (EMCV). (**A**) After 24 h, cells were fixed and subjected to CLEM. Low resolution confocal microscopy images identifying transfected cells are shown on the top left. The area in the red box is shown in the corresponding EM image. Yellow arrow heads indicate DMVs. Insets at the bottom indicate zoomed-in regions. (**B**) DMVs within whole cell sections were counted and divided by cell area (μm^2). Graph shows average and SD from 4 different transfected cells. Cells expressing comparable level of HCV replicase were selected for EM analysis. Significance was calculated by a paired t-test. **, $p<0.01$. (**C**) Expression levels of NS4B and NS5A in transfected cells were determined by western blotting. (**D**) Lipidome analysis of HCV-induced DMVs. Extracts of Huh7 cells containing the subgenomic replicon sg4B^{HA}31R (NS4B-HA) and Huh7 cells stably overexpressing HA-tagged Calnexin (CNX-HA) and control Huh7 cells were prepared as described in supplementary methods and used for HA-affinity purification under native conditions. An aliquot of the sample was analyzed by electron microscopy (top panels) whereas the majority was subjected to lipidome analysis by using mass spectrometry. Values obtained for the NS4B-HA sample were normalized to those obtained for the CNX-HA sample that was set to one. The complete list of analyzed lipids is summarized in data S3. (**E**) PA accumulation at NS5A containing structures. Huh7-Lunet/T7 cells were transfected with a construct analogous to the one in panel A, but containing a mCherry insertion in lieu of GFP, along with an EGFP-tagged wildtype (WT) or mutant (4E) PA sensor (construct pTM-EGFP-PABD-Raf1-WT or -4E). Twenty-four hours later, GFP-PABD and NS5A-mCherry were visualized by fluorescence microscopy. White boxes indicate regions magnified in the lower right of each panel. (**F**) Top panel: Alternate PA biosynthesis pathways via lysophosphatidic acid (LPA) or phosphatidylcholine (PC) catalyzed by AGPATs or PLDs, respectively. Bottom panel: Huh7-Lunet/T7 cells were electroporated with in vitro transcripts of a subgenomic HCV reporter replicon encoding the firefly luciferase. Four hours after transfection, different concentrations of PA synthesis inhibitors were added to the cells and luciferase activities were analyzed at 48 h after electroporation. Graph shows average and SD from 3 independent experiments. Cell viability determined by CellTiter-Glo luminescent assay is indicated with the red line. (**G**) PA recruitment to autophagy-related structures in selective and non-selective autophagy. Top panel: Huh7-derived cells expressing EGFP-PABD-Raf-1 were incubated in growth medium (top left panels) or in serum-free medium with 200 nM BafA1 (top right panels) for 3 h. Cells were fixed and stained with a LC3 specific antibody. Bottom panel: For selective autophagy, mCherry-tagged Parkin was co-expressed with EGFP-PABD-Raf1, followed by incubation with 10 µM Valinomycin to induce mitophagy. Cells were fixed after 3 h, and GFP-PABD and mCherry-Parkin were visualized by fluorescence microscopy. Images in panels E and G are maximum intensity projections.

bioRxiv preprint doi: https://doi.org/10.1101/2021.05.10.443480; this version posted May 10, 2021. The copyright holder for this preprint (which was not certified by peer review) is the author/funder. All rights reserved. No reuse allowed without permission.

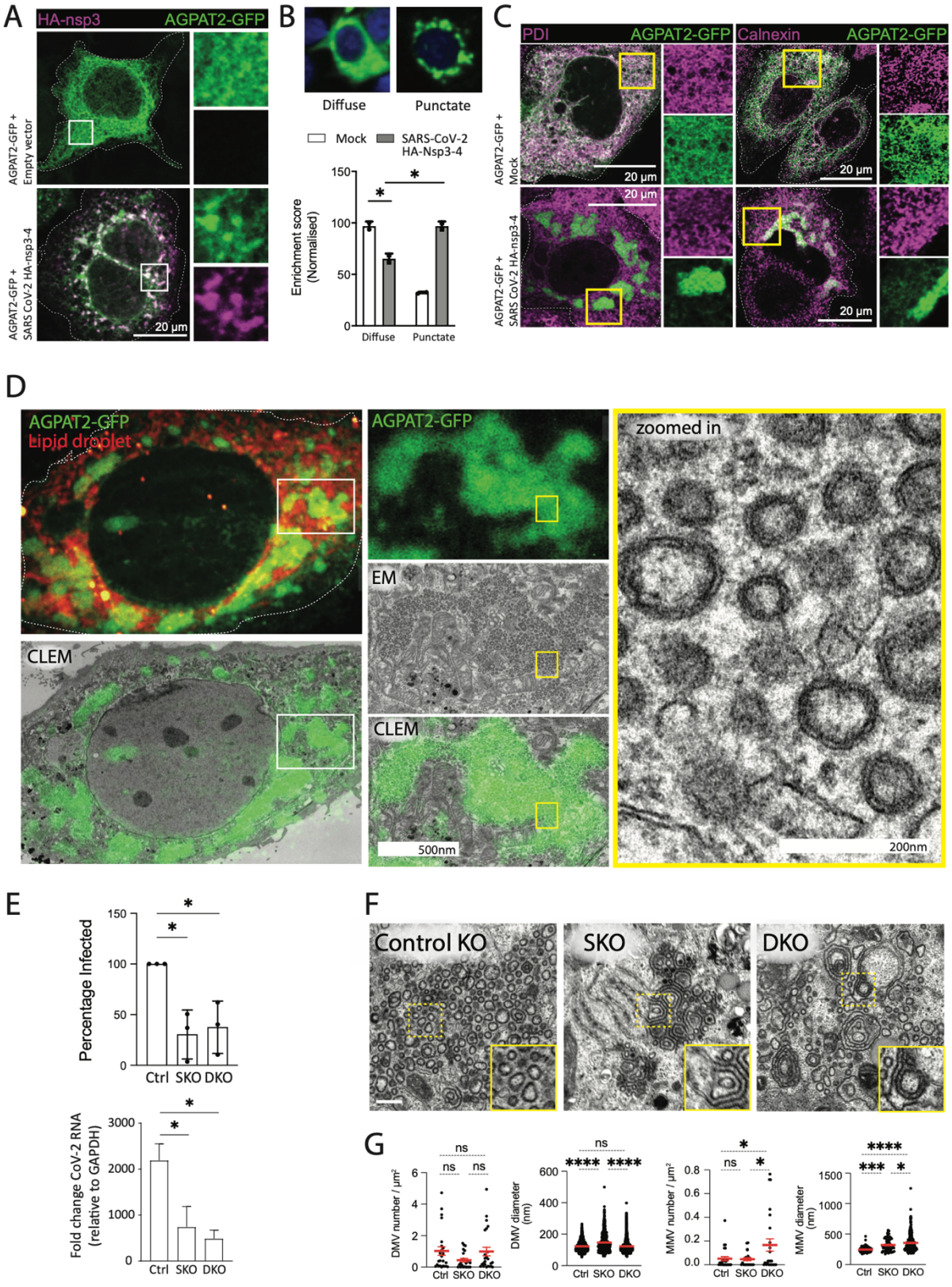

Fig. 3. AGPATs are recruited to SARS-CoV-2 induced DMVs and contribute to viral replication

(A) Change of subcellular localization of AGPATs upon expression of SARS-CoV-2 nsp3-4. Huh7-derived cells transiently expressing AGPAT2-GFP were transfected with a SARS-CoV-2 HA-nsp3-4-V5 expression construct or the empty vector. After 48h, cells were stained

bioRxiv preprint doi: https://doi.org/10.1101/2021.05.10.443480; this version posted May 10, 2021. The copyright holder for this preprint (which was not certified by peer review) is the author/funder. All rights reserved. No reuse allowed without permission.

with HA-specific antibody and examined by confocal microscopy. Maximum intensity projections are shown. Enrichment score indicates the likelihood of cells showing a punctate or diffuse staining pattern. (**B**) Clustering of AGPAT2-GFP in SARS-CoV-2 HA-nsp3-4-V5 expressing cells. Huh7-Lunet/T7 cells were co-transfected with AGPAT2-GFP and SARS-CoV-2 HA-nsp3-4-V5 or the empty vector. Twenty-four hours later, cells were fixed and ~1000 cells per condition were separated into two morphotypes (diffuse or punctate) using CellProfiler Analyst based semi-supervised classifier. Significance was calculated using an unpaired t-test. *, $p<0.05$. (**C**) AGPAT clustering occurs independent of ER remodeling induced by nsp3-4. Huh7-Lunet cells expressing AGPAT2-GFP and HA-nsp3-4-V5 were stained for the ER markers protein disulfide isomerase (PDI) and calnexin and analyzed by confocal microscopy. (**D**) AGPATs are localized at SARS-CoV-2 HA-nsp3-4-V5 induced DMVs. Huh7-derived cells were transiently transfected with AGPAT2-GFP HA-nsp3-4-V5 and subjected to CLEM. Light and EM images were correlated by using lipid droplets as fiducial markers. White and yellow boxes indicate areas magnified in the corresponding panels on the right. (**E**) AGPAT1/2 contribute to SARS-CoV-2 replication. Huh7-Lunet control, AGPAT2 single (SKO) and AGPAT1/2 double (D)KO cells were infected with SARS-CoV-2 (MOI=0.1). Twenty-four hours later, cells were fixed and immunostained for nucleocapsid, and the percentage of N-positive cells was determined using CellProfiler. Normalized data from three biologically independent experiments are plotted (top right panel). Total RNA was isolated from infected cells, and SARS-CoV-2 RNA levels were determined using RT-qPCR. Data were normalized to cellular GAPDH mRNA (bottom right panel). Significance was calculated using ordinary one-way ANOVA. *, $p<0.05$. (**F**) Aberrant SARS-CoV-2 DMVs in AGPAT1/2 DKO cells. Huh7-Lunet cells with single (SKO) or double knock-out (DKO) and stably expressing T7 polymerase were transfected with a plasmid encoding SARS-CoV-2 HA-nsp3-4-V5 and fluorescent neon-green. Twenty-four hours later, cells were fixed and NeonGreen positive cells were recorded and examined by EM. HA-nsp3-4-V5 induced DMVs and multi-membrane vesicles (MMVs) were quantified. Shown are the number and diameter of DMVs and MMVs in these cells as observed from at least 8 cell profiles per condition. Statistical significance was calculated using ordinary one-way ANOVA. ****, $p<0.001$. Light microscopy images in panels A to D are maximum intensity projections.

bioRxiv preprint doi: https://doi.org/10.1101/2021.05.10.443480; this version posted May 10, 2021. The copyright holder for this preprint (which was not certified by peer review) is the author/funder. All rights reserved. No reuse allowed without permission.

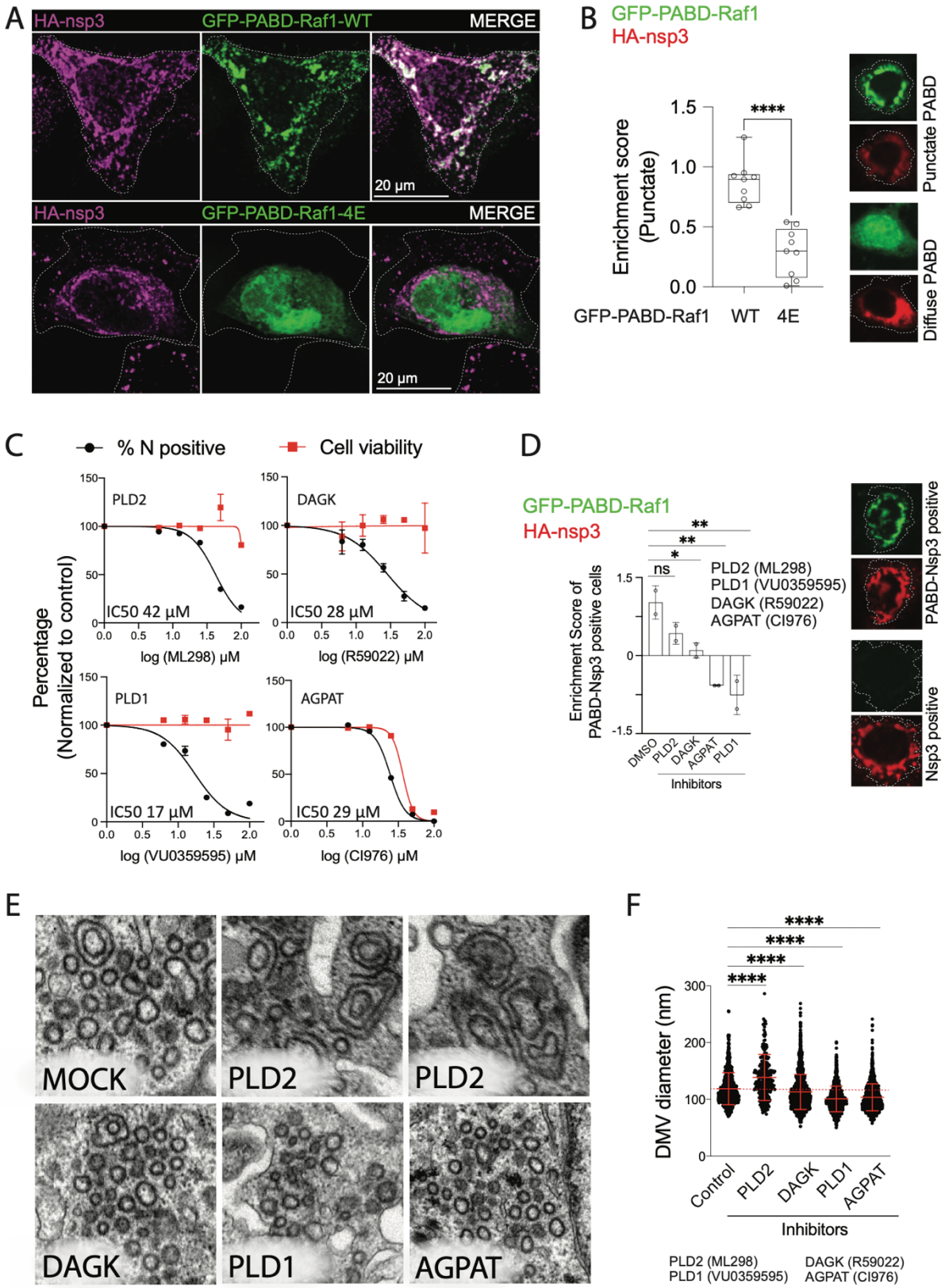

Fig. 4. PA accumulation at SARS-CoV-2 DMVs and role of alternative PA synthesis pathways for SARS-CoV-2 replication and DMV formation. (**A**) PA enrichment at SARS-CoV-2 nsp3-containing structures. Huh7-Lunet cells expressing the wildtype or mutant form of the PA sensor were transfected with the plasmid encoding HA-nsp3-4-V5 and

bioRxiv preprint doi: https://doi.org/10.1101/2021.05.10.443480; this version posted May 10, 2021. The copyright holder for this preprint (which was not certified by peer review) is the author/funder. All rights reserved. No reuse allowed without permission.

679 24 h later, cells were fixed, immunostained with HA-specific antibody and HA-nsp3 and
680 GFP-PABD were visualized by confocal microscopy. Maximum intensity projections are
681 shown. (**B**) Using CellProfiler Analyst, a semi-supervised machine learning classifier was
682 trained to differentiate between punctate and diffuse signals of the GFP-PABD sensor (top
683 panel). A normalized enrichment score which indicates the probability of cells showing
684 punctate GFP-PABD localization to nsp3 fluorescent signal across the whole cell population
685 is shown in the graph on the bottom panel. Significance was calculated by unpaired t-test.
686 ****, $p<0.0001$. (**C**) Alternative pathways for PA generation are important for SARS-CoV-2
687 replication. Calu-3 cells were infected with SARS-CoV-2 (MOI=5) in the presence of
688 AGPAT, PLD1/2, or DAGK inhibitors. Cells were fixed 24 h post infection, stained with
689 nucleocapsid-specific antibody and percentage of infected cells was quantified using
690 CellProfiler. Cell viability and percentage inhibition are plotted as dose-response curves and
691 IC50 values are given on the top of each panel. (**D**) AGPAT, PLD and DAGK inhibitors
692 reduce PA accumulation at nsp3-positive structures. Huh7-Lunet cells were transfected with
693 SARS-CoV-2 HA-nsp3-4-V5 and GFP-PABD-Raf1 encoding plasmids, followed by addition
694 of a given inhibitor 4h after transfection. Twenty-four hours later, cells were fixed and HA-
695 nsp3 was detected with an HA-specific antibody. GFP-PABD and HA-nsp3 were visualized
696 by confocal microscopy. A semi-automated machine learning based classifier was trained to
697 separate HA-nsp3/PABD double-positive structures from HA-nsp3 single positive structures.
698 Enrichment score for HA-nsp3/PABD double-positive structures showing the up or
699 downregulation of double positive cells in different samples is plotted and statistical
700 significance was calculated using ordinary one-way ANOVA. *, $p<0.05$, **, $p<0.005$. (**E**)
701 Decrease of SARS-CoV-2 DMV diameter by AGPAT, PLD and DAGK inhibitors. Huh7-
702 Lunet/T7 cells were transfected with the plasmid encoding HA-nsp3-4-V5 and fluorescent
703 NeonGreen, followed by addition of inhibitors 4 h after transfection. Twenty-four hours later,
704 cells were fixed, NeonGreen positive cells were recorded and examined by EM.
705 Representative images are shown for each condition. (**F**) Number and morphology of DMVs
706 were determined for at least 7 cell profiles per condition. DMV diameters are plotted and
707 statistical significance was calculated using ordinary one-way ANOVA. ****, $p<0.001$.